Dark Current Suppression during High Speed Photogate Modulation for 3D ToF Imaging Pixel

Tae-Yon Lee[1], YongJei Lee[1], Dong-Ki Min[1], Joonho Lee[1], Young-Gu Jin[1], Yoondong Park[1], and Chilhee Chung[1]
Ilia Ovsiannikov[2] and Eric R. Fossum[1,2]

[1]Semiconductor R&D Center, Samsung Electronics, Yong-In, Kyonggi, South Korea
[2]Samsung Semiconductor Inc., Pasadena, CA, USA
* e-mail: taeyon.lee@samsung.com, Tel.: +82-31-209-6352, Fax.: +82-31-209-6300

A pair of photogates is employed as a high frequency demodulation pixel for three dimensional time-of-flight image sensor. Using a 192×108 array of the pixels, demodulation contrast above 50% is achieved at 20MHz frequency and the test chip exhibits distance error less than 1% up to 7 m detection of the object. Modulation frequency dependent behavior of dark current is observed: dark current is reduced as the photogate modulation frequency increases. One possible interpretation is quenching of interface traps under the photogate by carriers from the bridging diffusion especially at reduced temperature.

Significant research efforts have been made to realize all-solid-state three dimensional (3D) image sensor. One approach is to use the time-of-flight (ToF) method in which the distance is measured by the phase delay of reflected light. The phase delay is extracted by demodulation of the continuously modulated optical power after reflection from the object.[1-3]

Demodulation performance at high modulation frequency (f) is a prerequisite for small-distance error (DE) measured over large distance range. In addition, large signal-to-noise ratio is essential to reduce DE from the modulated invisible infrared (IR) light irradiation. A pixel design employing the classic 5T photogate structure [4] satisfies such requirements. We report a 3D ranging image sensor using a pixel with photogate structure with bridging diffusion (BD) and correlated double-sampling (CDS). We observe that suppression of dark current occurs as modulation frequency of photogate increases.

Figure 1 shows the schematic pixel structure of the demodulation pixel, comprised of photogate pair (PG_A/PG_B). Each half, in classic single-poly 5T photogate style [4], has a BD, transfer-gate (TG), FD, and reset gate (RG), as well as its own output source-follower and select transistor. This allows full CDS for readout since the signal can be integrated under the photogate and BD even during modulation. In addition, BD helps charge transfer from photodiode to FD.

The feasibility of the demodulation operation of the pixel is checked by 3D technology computer aided design simulation, in consideration of pixel geometry, doping profile, and bias condition. Figure 2 shows the calculated cross-sectional potential profile of our pixel, where 3.0 and 0.0 V bias' are applied to PG_A and PG_B, respectively. It is clearly shown that distinctive depletion volume under each PG is generated. This indicates that our pixel can work as a ToF demodulator effectively.

A test chip was fabricated using a 0.13 μm CMOS image sensor process. Photodiode is formed on a lightly doped p-type epitaxial layer, grown on a highly doped p-substrate. A conventional p- and n- doping profile usually adopted in modern CMOS image sensor is employed. The 192×108 array of the pixels, along with decoder and drivers for rows/columns as well as for CDS comprise the chip, as shown in the die photo Fig.3. For signal

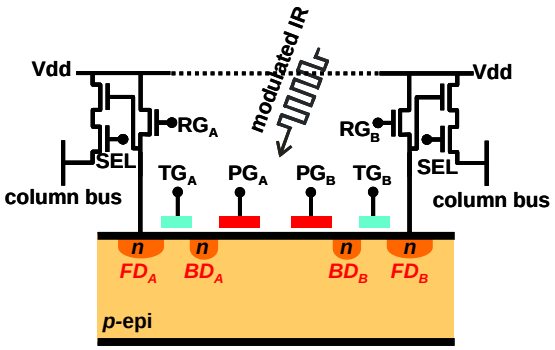

Fig.1 Schematic cross-section of a pixel composed with photogates PG_A/PG_B and accompanying BD, TG, FD, RG, source follower and selection transistor (SEL).

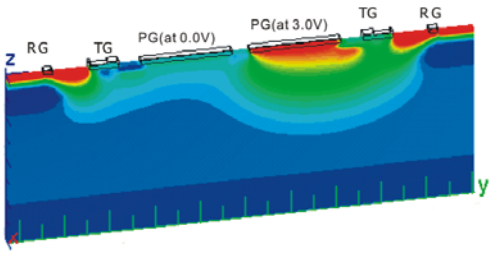

Fig.2 Calculated cross-sectional potential profile of the pixel, accompanying pair of PG, TG, BD, RG, and FD. PGs in left- and right- hand are at bias of 0.0 and 3.0 V, respectively. The BD is located between PG and TG, and FD is located between TG and RG.

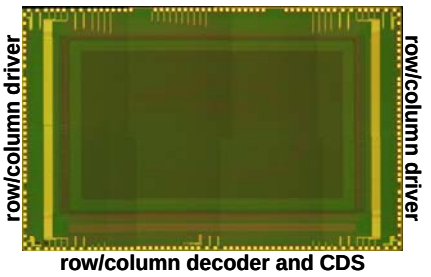

Fig.3 Photo of a ToF 3D image sensor chip composed of 192×108 array of pixels along with decoder and drivers for rows/columns as well as for CDS, and input/output pins.

processing, CDS and readout circuitary similar to those in Ref[4] is adopted.

Functionality and performance of our chip as a demodulator are characterized with an 850 nm LED operated as a square-wave-modulated light source. The image is obtained with rolling-shutter timing with the analog signal digitized by an off-chip 12-bit ADC. Both LED and photogates toggle with periodicity T (T=1/f) which is much shorter than the integration time. During integration, biases to PG_A and PG_B are modulated out-of-phase (T/2 or 180^o phase difference) from each other. After integration, reset level and signal level are readout in the standard way. The resulting signals are denoted as sig_0 and sig_{180}, respectively. The phases of the modulation gates are then T/4 or 90^o adjusted and a second integration is performed to obtain sig_{90} and sig_{270} as a result. In this study, a pseudo-single tap operation was used to eliminate any minor difference of the left-and-right hand side, so that a third and fourth integrations with T/2 and 3T/4 modulation shift of photogates are required to obtain sig_{180} and sig_{270}.

The distance R is determined from these four signals with following equation:

$$R = \frac{c}{4\pi f} \cdot \tan^{-1}\left(\frac{sig_0 - sig_{180}}{sig_{90} - sig_{270}}\right) \qquad (1)$$

where c is the speed of light.

Figure 4 shows dependence of extracted R using Eq.(1) and distance error on real distance measured under the same LED power irradiation. Good linearity between real distance and measured distance up to 7 m is confirmed. Distance error is less than 1% up to 7 m distance. Such noticeable performance is possible due to relatively high demodulation contrast, more than 50% at 20MHz, reasonable quantum efficiency, and signal-to-noise ratio. It is noted that DE increases as real distance increases. This can be attributed to the increasing contribution of noise and background signal as the reflected optical power becomes reduced at far distance.

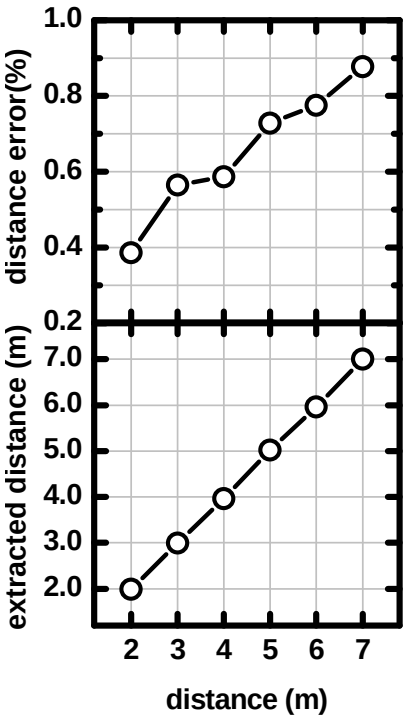

Fig.4 Extracted distance and distance error measured between 1 and 7 m distance with 20 MHz demodulation frequency and 10 msec integration. The F number was 1.2, and LED illuminance was kept as 400 mW over the whole measurement.

Dark current can degrade demodulation performance [2,3,5]. For a pixel employing a photogate, interface traps are likely as a dark-current source due to the unpinned nature of the photogate structure. On this regard, dark current was examined more carefully. For various modulation frequencies, dark signal is obtained in temperature range between 30 and 80^{o}C for various integration time. Dark current is obtained from the slope of dark offset *vs.* integration time curves.

Figure 5 shows Ahrrenius relation, dependence of dark current on the inverse temperature, whose slope, E_a, can be interpreted as "average" energy over a spectrum of interface traps and exhibits characteristic thermal activation process contributing to dark current: In general, E_a of 1.12 eV corresponds to bulk-diffusion-limited dark current. Interface-trap-limited case exhibits reduced val-

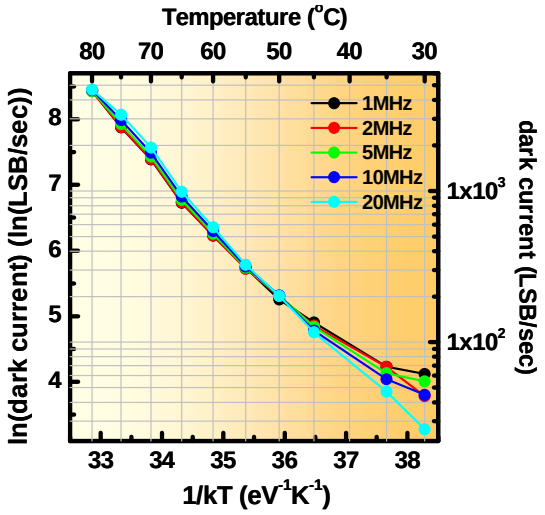

Fig.5 Ahrrenius relation from temperature dependence of dark current, obtained for various demodulation frequency. Dark current is obtained from the slope of dark offset *vs.* integration time curve. Dark current is suppressed as photogate modulation frequency increases below 50°C, above which the effect of dark current suppression becomes smaller.

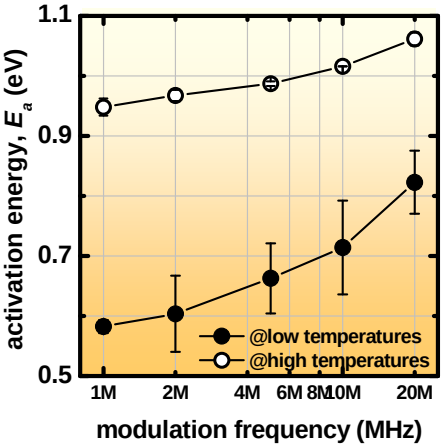

Fig.6 Frequency dependence of thermal activation energy, from the Ahrrenius relation between dark current and inverse temperature in Fig.5. The activation enenergies are obtained from low temperature range between 30 and 50°C, and high temperature range between 50 and 65°C, respectively. Error-bar is obtained from the linear fitting procedure.

ue.[6]

It is noted that Fig. 5 exibits two distinctive temperature ranges, in which the magnitude of dark current and thermal activation energy (E_a) shows different dependence on demodulation frequency. Below 50°C, dark current is suppressed at higher modulation frequencies. On the other hand, this suppression effect becomes reduced or inverted as temperature increases above 50°C.

Dependence of E_a on modulation frequency for the two temperature ranges is collected in Fig. 6. At low temperature range, E_a increases from 0.58 eV at 1 MHz to 0.82 eV at 20 MHz. Increase of E_a with increasing frequency suggests that fewer traps in the bandgap participate. A likely source of dark current is from traps under PG. During one half of the modulation period $T/2$, electrons can flow from the bridging diffusion to under the photogate forming a quenching layer of electrons that occupy traps but do not pin the interface potential. At higher frequencies, the deeper traps do not have enough time to emit the captured charge carriers during the second half of the modulation period and their contribution to dark current is effectively quenched. On the other hand, E_a significantly increases as 0.95 eV at 1 MHz, and 1.06 eV at 20 MHz, respectively. This indicates that contribution from the interface trap becomes smaller due to the enough thermal energy, especially when the modulation period becomes elongated, or modulation frequencie becomes smaller at higher temperature.

The demodulation performance of our pixel is reflected in the measured 3D images, as shown in Fig.7. To obtain a 3D image, four consecutive 2D images, corresponding to sig_0, sig_{90}, sig_{180}, and sig_{270}, were measured (pseudo-single tap operation) by a custom-built camera which employs our pixel array. Figure 7 (a) shows 2D image of a statue at 1 m distance from the camera, obtained from sig_0. Figure 7 (b) shows 3D image, after image signal processing using Eq.(1). It is visible that Fig.7 (b) resolves exact distance information, which is in agreement with the result in Fig. 4; For a statue located at 1 m distance, depth information with a few cm resolution could be resolved. Thus, it is interpreted that our pixel suffices requirement for 3D imager with enough distance resolution.

In summary, photogate pixel for 3D ToF demodulation sensor is successfully demonstrated. The major 3D as well as 2D performance parameters of the pixel show reasonable values for acquisition of 3D as well as 2D images. Dark current becomes suppressed as modulation frequency of photogate increases, especially at reduced temperature range. This effect is interpreted as effective quenching of charge emission from the interface, *e.g.* at BD and the underneath of PG. Still, contribution from other interfaces cannot be excluded, and detailed study should be carried out. It is concluded that adoption of

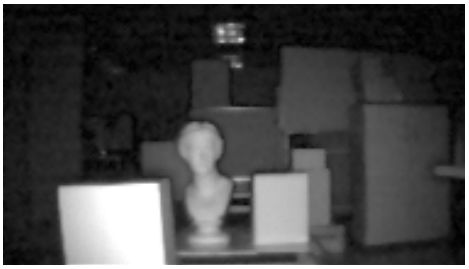

(a)

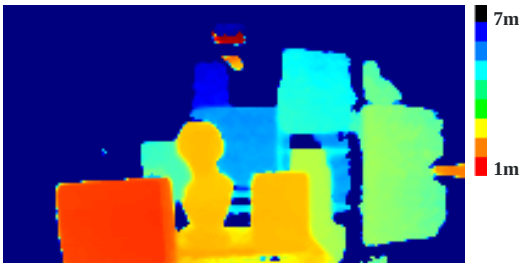

(b)

Fig.7 Images of various objects located at distance between 1 and 7 m, obtained with the custom built camera under the conditions of modulating LED exposure with 200 mW illuminance and 10 msec integration time. In (a) a raw 2D image corresponds to sig_0 is shown. In (b), a fully processed 3D image is shown. Color level scales with the distance from the camera surface.

photo-gate as a demodulation pixel can be a competitibe choice for fabrication of 3D ToF image sensor. More tuned pixel structure along with advanced noise reduction algorithm, employment of low noise read circuit will facilitate more promising 3D imaging solution.

References:

[1] R. Lange, P. Seitz, A. Biber, and S. Lauxtermann, "Demodulation Pixels in CCD and CMOS Technologies for Time-of-Flight Ranging", Proceeding of the SPIE, vol. 3965A, p. 177 (2000)

[2] S.B. Gokturk, H. Yalcin, and C. Bamji, "A Time-of-Flight Depth Sensor-System Description, Issues and Solutions", Proceeding of Computer Vision and Patterns Recognition 2004, vol.3, p.35 (2004)

[3] T. Möller, H. Kraft, J. Frey, M. Albrecht, and R. Lange, "Robust 3D Measurement with PMD Sensors", Proceedings of the 1st Range Imaging Research Days at ETH Zurich (2005)

[4] S.K. Mendis, S.E. Kemeny, R.C. Gee, B. Pain, C.O. Staller, Q. Kim, and E.R. Fossum,"CMOS Active Pixel Image Sensors for Highly Integrated Imaging Systems," IEEE Journal of Solid State Circuits, vol. 32, p. 187 (1997).

[5] B. Büttgen, T. Oggier, M. Lehmann, R. Kaufmann, and F. Lustenberger, "CCD/CMOS Lock-In Pixel for Range Imaging: Challenges, Limitations and State-of-the-Art", Proceedings of the 1st Range Imaging Research Days at ETH Zurich (2005)

[6] J. Nakamura, "Basics of Image Sensors", *Chap.3 in Image Sensors and Signal Processing for Digital Still Cameras*, edited by J. Nakamura (Taylor & Francis Group, Boca Raton), 2006